ELSEVIER

Physica E 8 (2000) 333–341

PHYSICA E

www.elsevier.nl/locate/physe

# Interband absorption and luminescence in small quantum dots under strong magnetic fields

Augusto Gonzalez[a,b,*], Eduardo Menéndez-Proupin[c]

[a] *Centro de Matemáticas y Física Teórica, Calle E No. 309, Ciudad Habana, Cuba*
[b] *Departamento de Física, Universidad de Antioquia, AA 1226, Medellin, Colombia*
[c] *Instituto de Materiales y Reactivos, Universidad de La Habana San Lázaro y L, Vedado 10400, Ciudad Habana, Cuba*

Received 5 March 2000; accepted 25 April 2000

**Abstract**

Interband absorption and luminescence of quasi-two-dimensional, circularly symmetric, $N_e$-electron quantum dots are studied at high magnetic fields, $8 \leqslant B \leqslant 60$ T, and low temperatures, $T \ll 2$ K. In the $N_e = 0$ and 1 dots, the initial and final states of such processes are fixed, and thus the dependence on $B$ of peak intensities is monotonic. For larger systems, ground state rearrangements with varying magnetic field lead to substantial modifications of the absorption and luminescence spectra. Collective effects are seen in the $N_e = 2$ and 3 dots at "filling fractions" $\frac{1}{2}$, $\frac{1}{3}$ and $\frac{1}{5}$. 

*PACS:* 71.35.Ee; 78.66.−w

*Keywords:* Quantum dots; Electron–hole systems; High magnetic fields

## 1. Introduction

The quasi-two-dimensional electron gas in a high magnetic field is a strongly correlated system exhibiting very complicated dynamics. At special values of the filling factor, the essential features of the ground state are captured by the Laughlin wave function [1], or its composite fermion generalization [2]. The low-lying excitations can be described in the single-mode approximation of Girvin et al. [3,4] or in the composite fermion picture [2,5,6].

Many experiments have been designed and carried out in order to test the excitation spectrum of this highly correlated system. Inelastic (Raman) light scattering experiments have tested basically the excitation gap at wave vector $\boldsymbol{k} = 0$ [7–10]. Spin-flipped states and the magnetoroton minimum at $k \approx 1/l_B$ ($l_B$ is the magnetic length) have also been observed, although they should be activated by impurities or other mechanism to produce a trace in the Raman

* Correspondence address: Departamento de Física, Universidad de Antioquia, AA 1226, Medellin, Colombia.
*E-mail addresses:* agonzale@cidet.icmf.inf.cu (A. Gonzalez), earicl@ff.oc.uh.cu (E. Menéndez-Proupin).

1386-9477/00/$ - see front matter 
PII: S1386-9477(00)00156-9

spectra. Evidence of the magnetoroton minimum comes also from the absorption of ballistic acoustic phonons [11,12].

On the other hand, experiments on photoluminescence (PL) related to interband electronic transitions around filling factor $\nu = 1$ have tested the excited states with an additional electron–hole (e–h) pair [13–16]. Recently, the observations have been extended to lower filling factors by increasing the magnetic field up to 60 T [17,18]. The related theory is not in complete agreement with the experiment. In the infinite magnetic field limit, it was predicted that only the exciton ($X^0$) and the negatively charged triplet exciton ($X_t^-$) are bound [19]. The latter is expected to be dark in luminescence [19] as a result of a hidden symmetry related to magnetic translations [20]. In the experiments, however, very distinct singlet and triplet peaks ($X_s^-$ and $X_t^-$) are observed. A realistic calculation of ground state energies was presented in Ref. [21], where Landau level and quantum well (qwell) sub-band mixing were taken into account. The $X_t^-$ peak position was reproduced, but in theory this state is dark. The problem was recently revisited by Wojs et al. [22], who showed that in a narrow (10 nm wide) well a second bright $X_t^-$ state becomes bound, thus interpreting the observed luminescence as coming from the bright state. We shall notice that both Refs. [21,22] deal with isolated three-particle systems, and thus are not able to describe the filling factor dependence of observed magnitudes for $\nu \geqslant \frac{1}{5}$.

In the present paper, we study small quantum dots (qdots) under conditions similar to the experiments reported in Refs. [17,18], i.e. quasi-two-dimensional motion, magnetic fields in the interval $8\,\mathrm{T} \leqslant B \leqslant 60\,\mathrm{T}$, and temperatures well below 2 K. The laser excitation power is assumed to be low (a few $\mathrm{mW/cm^2}$), thus the dot works under a linear regime. The lateral confinement is modelled by a harmonic potential. Energy levels, charge densities and dipole matrix elements for absorption and luminescence are computed by exact diagonalization in the first Landau level (1LL) approximation.

Absorption or PL experiments on electron–hole qdots under very high magnetic fields are lacking. To the best of our knowledge, there is only one experiment [23] in which the luminescence at higher (4 K) temperature and $B \leqslant 45\,\mathrm{T}$ is measured in order to estimate the e–h correlation energy.

Breaking of the magnetic translation symmetry by a lateral confinement in a qdot makes the lowest $X^-$ triplet state bright. Highly nontrivial PL and absorption spectra arise even in the 1LL approximation. These spectra contain information about the energy levels and particle correlations in the system. Let us stress that a calculation of $X^0$ and $X^-$ energy levels in a qdot, which includes LL mixing, is available [24]. The absorption coefficient is also reported in that paper. The differences with our work are the following. First, we consider both absorption and PL. Second, we trace the changes in the ground-state (g.s.) wave function and charge rearrangements as the magnetic field is varied. Finally, we consider larger qdots with $X^{2-}$ and $X^{3-}$ complexes (unbound in a qwell). It will be seen below that indications of collective effects are evident even in these relatively small systems.

The plan of the paper is as follows. The model and certain general statements are explained in Section 2. The next section presents results for particular systems. We start with the exciton and end up with the $X^{3-}$ complex. Finally, a few concluding remarks are given.

## 2. The model

We consider the two-dimensional motion of $N_e$ electrons and $N_h$ holes in an external parabolic potential and a perpendicular magnetic field (along the $z$-axis). In particular, we will study the $N_h = 1$ and 0 systems, which are the ones participating in interband absorption and recombination processes. The unit of length is $\sqrt{2}$ times the magnetic length. In the 1LL approximation, the Hamiltonian is written as

$$H(N_e, N_h) = \left(\frac{\hbar\omega_c^e}{2} + E_z^e\right) N_e + \left(\frac{\hbar\omega_c^h}{2} + E_z^h + E_{gap}\right) N_h + E_{Zeeman}^e + E_{Zeeman}^h + V_{conf} + V_{coul}. \quad (1)$$

Hamiltonian (1) is intended to model a GaAs qdot with a thickness of 20 nm in the $z$-direction. The meaning of the different terms entering $H$ is evident. The specific qdot characteristics are reflected in the confinement energies along the $z$-direction, $E_z$, the in-plane confinement potential, $V_{conf} = \sum_i v_{conf}(r_i)$, and the $z$-averaged Coulomb interactions, $V_{coul} =$

$\sum_{i,j} v_{\mathrm{coul}}(r_{ij})$. We will use the expression

$$v_{\mathrm{coul}}(r) = \pm 3.316\ \beta\sqrt{B}\,\frac{1}{r}\ (\mathrm{meV}), \tag{2}$$

for the pair Coulomb interactions ($B$ in Teslas), and

$$v_{\mathrm{conf}}(r) = \frac{3.316}{B}\beta K r^2\ (\mathrm{meV}), \tag{3}$$

for the one-particle confinement potential. Even these simple expressions lead to very interesting physical results. Notice that $1\sqrt{2}$ times the characteristic Coulomb energy, $e^2/(\kappa l_{\mathrm{B}})$, equals $3.316\ \sqrt{B}$ in our units. The constant $\beta = 0.6$ is used to simulate the $z$-averaging of the Coulomb interactions in the 20 nm-wide qdot [4,25]. We fixed it by requiring the binding energy of the unconfined ($v_{\mathrm{conf}}$ set to zero) $X_{\mathrm{t}}^-$ relative to the $X^0$ to be 0.6 meV at $B = 17$ T. This is a representative value [18]. On the other hand, the dimensionless constant $K$ will be fixed to 7.0 in order to obtain a "filling factor" around $\frac{1}{3}$ for $B \approx 30$ T, also a common situation met in the experiments [18].

The only nontrivial terms entering Eq. (1) are $V_{\mathrm{conf}}$ and $V_{\mathrm{coul}}$. They should be diagonalized in a basis of Slater 1LL functions. The energies coming from the diagonalization processes will be denoted $\varepsilon$, and the wave functions will be used to compute physical observables. Note that, in the 1LL, the electron (hole) angular momentum is a non-positive (non-negative) number. Thus, the total angular momentum is written $M = M_{\mathrm{e}} + M_{\mathrm{h}} = -|M_{\mathrm{e}}| + M_{\mathrm{h}}$.

In a GaAs electron system, the validity of the 1LL approximation can be stated by comparing the excitation energy to the 2LL, $\hbar\omega_c^{\mathrm{e}} = 1.728B$ meV, with the Coulomb energy, $3.316\beta\sqrt{B}$ meV. Thus, for $B \gg 1$ T the 1LL approximation works. Spin excitations are lower in energy, $\Delta E_{\mathrm{Zeeman}} \approx 0.025B$ meV. However, at temperatures below 2 K and for $B > 8$ T, they cannot be thermally excited. It means that in both absorption and luminescence the transition starts from the lowest optically active state. When holes are created, the 1LL approximation becomes valid at higher fields. If we take for the heavy hole mass in the $xy$ plane the value $\mu_{\mathrm{h}} = 0.11m_0$ [26], then $\hbar\omega_c^{\mathrm{h}} \approx 1B$ meV. The 1LL approximation works for $B \gg 4$ T. Below, we present results obtained in the 1LL approximation for $8\ \mathrm{T} \leqslant B \leqslant 60$ T.

On the other hand, expression (1) assumes that the particles are sitting on the first qwell sub-band. As it was stressed in Ref. [21], this may be a rough approximation. For a 20 nm qwell, the second electronic sub-band is around 30 meV higher, but the second hole sub-band is only 6 meV higher (a heavy hole mass $\mu_{\mathrm{h}}^z \approx 0.38m_0$ is assumed). Our first sub-band approximation is qualitatively valid in the present situation, and will improve for narrower wells.

### 2.1. Interband absorption and luminescence (general grounds)

Interband absorption and luminescence will be studied at temperatures $T \ll 2$ K, i.e. typically lower than spin excitation gaps. Thus, the processes proceed from a unique initial state, which is the g.s. of the polarized ($N_{\mathrm{e}}$, 0) system in absorption, and the lowest optically active state of the ($N_{\mathrm{e}} + 1$, 1) system in emission. In general, these processes take place in different angular momentum channels. For absorption, the incident light is supposed to be circularly polarized and propagating along the $z$-direction. Also circularly polarized light is supposed to be measured from the qdot luminescence.

A simple two-band model, with bands split by the Zeeman energy, will be used. The conduction-band ($m_{\mathrm{s}} = \pm\frac{1}{2}$) mass is $\mu_{\mathrm{e}} = 0.067m_0$, and the heavy hole band, $m_j = \pm\frac{3}{2}$, shows anisotropic effective masses, $\mu_{\mathrm{h}} = \mu_{\mathrm{h}}^{xy} = 0.11\ m_0$, $\mu_{\mathrm{h}}^z = 0.38m_0$. LL mixing in the $m_j = \frac{3}{2}$ branch [27] will be neglected. $m_j = -\frac{3}{2}$ will be called the spin-up hole branch, and $m_j = \frac{3}{2}$ – the spin-down branch. For propagation along the $z$-axis, the allowed transitions are $m_j = -\frac{3}{2} \to m_s = -\frac{1}{2}$ for right-handed circular polarization (RHCP), and $m_j = \frac{3}{2} \to m_s = \frac{1}{2}$ for left-handed circular polarization (LHCP) [27,28].

The dipole approximation is used for the interaction Hamiltonian, i.e. $-\mathscr{E}\cdot\boldsymbol{D}$. In the 1LL, the interband dipole operator takes the form

$$\boldsymbol{D} = \frac{\mathrm{e}\boldsymbol{p}_{\mathrm{cv}}}{m_0\omega}\sum_{l\geqslant 0}\left(e_{-l,\downarrow}^{\dagger}h_{l,\uparrow}^{\dagger} + e_{-l,\uparrow}^{\dagger}h_{l,\downarrow}^{\dagger}\right) + \mathrm{h.c.}, \tag{4}$$

where $\boldsymbol{p}_{\mathrm{cv}}$ is the GaAs interband constant. The reason for not including the light hole in Eq. (4) is twofold. First $E_z$ is around 6 meV higher ($\mu_{\mathrm{lh}}^z \approx 0.09m_0$), thus its absorption or luminescence lines are shifted. Second, the constant $\boldsymbol{p}_{\mathrm{cv}}^2$ is three times smaller for light holes. Notice that the interaction Hamiltonian preserves total angular momentum.

In our $(N_e, N_h)$ systems with $N_h = 0,\ 1$, the states may be classified according to the symmetry of the electronic subsystem. For example, the $N_e = 2$ system may be in a spatially antisymmetric (triplet) state, or in a spatially symmetric (singlet) state. We will present calculations only for spatially antisymmetric states. They are the only ones appearing in LHCP, and the ones associated to the most intense lines in RHCP [24]. The wave functions may be written as $\psi = \phi^{\text{antisymm}}_{\text{coord}}\chi^{\text{symm}}_{\text{spin}}$, or in a second quantization formalism,

$$|\psi(N_e,0)\rangle = \sum C_{l_1 l_2 \ldots l_{N_e}} e^{\dagger}_{-l_1,\uparrow} e^{\dagger}_{-l_2,\uparrow} \cdots e^{\dagger}_{-l_{N_e},\uparrow}|0\rangle, \quad (5)$$

$$|\psi_{\text{LHCP}}(N_e+1,1)\rangle = \sum C_{l_1 l_2 \ldots, l_{N_e+1}, l_h} e^{\dagger}_{-l_1,\uparrow} e^{\dagger}_{-l_2,\uparrow} \cdots e^{\dagger}_{-l_{N_e+1},\uparrow} h^{\dagger}_{l_h,\downarrow}|0\rangle, \quad (6)$$

$$|\psi_{\text{RHCP}}(N_e+1,1)\rangle = \frac{1}{\sqrt{N_e}} \sum C_{l_1 l_2 \ldots l_{N_e+1}, l_h} \times (e^{\dagger}_{-l_1,\downarrow}, e^{\dagger}_{-l_2,\uparrow} \cdots e^{\dagger}_{-l_{N_e+1},\uparrow} + e^{\dagger}_{-l_1,\uparrow} e^{\dagger}_{-l_2,\downarrow} \cdots e^{\dagger}_{-l_{N_e+1},\uparrow} + \cdots + e^{\dagger}_{-l_1,\uparrow} e^{\dagger}_{-l_2,\uparrow} \cdots e^{\dagger}_{-l_{N_e+1},\downarrow}) h^{\dagger}_{l_h,\uparrow}|0\rangle. \quad (7)$$

$\psi_{\text{LHCP}}$ corresponds to a spin-polarized electronic sub-system, and $\psi_{\text{RHCP}}$ to a not completely polarized state. In the pure electron system, the sum runs over angular momentum states obeying $0 \leqslant l_1 < l_2 < \cdots < l_{N_e}$ and fixed $M = -l_1 - l_2 - \cdots - l_{N_e}$. In the one-hole system, the total angular momentum $M = -l_1 - l_2 - \cdots - l_{N_e+1} + l_h$ is fixed.

Diagonalization of $V_{\text{conf}} + V_{\text{coul}}$ in Eq. (1) leads to the determination of eigenenergies and wave functions. Transition energies, transition probabilities and charge densities of the relevant states are computed from these results. The transition energies are given by

$$\hbar\omega = E_{\text{gap}} + E^{e}_{z} + E^{h}_{z} + \frac{\hbar\omega^{e}_{c}}{2} + \frac{\hbar\omega^{h}_{c}}{2} + E^{e}_{\text{Zeeman}} + E^{h}_{\text{Zeeman}} + \varepsilon(N_e+1,1) - \varepsilon(N_e,0), \quad (8)$$

where $\varepsilon$ are the energies coming from $V_{\text{conf}} + V_{\text{coul}}$. We took the values $E_{\text{gap}} = 1510$, $E^{e}_{z} = 11, E^{h}_{z} = 2$, $\hbar\omega^{e}_{c}/2 = 0.864\ B$, $\hbar\omega^{h}_{c}/2 = 0.526B$, $E^{e}_{\text{Zeeman}} = -0.025 m^{e}_{s} B$, $E^{h}_{\text{Zeeman}} = -0.016 m^{h}_{s} B$, for the quantities entering Eq. (8), where energies are given in meV and $B$ in Teslas. Our treatment of Zeeman energies of both electrons and holes is very simple. We used the value $g_e = -0.44$ for the electron Landé factor and extracted the hole energy from the observed splitting of $X^0$ luminescence lines in RHCP and LHCP [18]. The hole spin projection is conventionally written as $m^{h}_{s} = \pm\frac{1}{2}$. Actually, the Zeeman energy shows a non-linear dependence on $B$ [29]. Notice, however, that $E_{\text{gap}}$, $\hbar\omega_c$ and $E_{\text{Zeeman}}$ are important in determining the absolute position of a given absorption or PL line, but not its relative position with respect to $X^0$ in the same polarization.

The absorption coefficient of a dot is given by

$$\alpha(\omega) = \frac{4\pi^2\omega}{\hbar c V} \sum_{f} |\langle f|\boldsymbol{e}\cdot\boldsymbol{D}|i\rangle|^2 \delta(\omega - \omega_{\text{fi}}), \quad (9)$$

where $|i\rangle$ is the g.s. of the $(N_e, 0)$ system, $f$ are the states of the $(N_e + 1,\ 1)$ system in the same angular momentum tower and $\hbar\omega_{\text{fi}}$ is their energy difference computed from (8). $\boldsymbol{e}$ is the light polarization vector, $c$ the light velocity, and $V$ is the volume of absorption. We have used a phenomenological width, $\Gamma = 0.8$ meV, to replace the delta function by a Lorentzian

$$\delta(x) \to \frac{\Gamma/\pi}{\Gamma^2 + x^2}. \quad (10)$$

In luminescence, we compute the matrix elements $|\langle f|\boldsymbol{e}\cdot\boldsymbol{D}|i\rangle|^2$, assuming that $|i\rangle$ is the lowest state of the $N_h = 1$ system.

## 3. Results

We present results in th following interval of magnetic field values, $8\ \text{T} \leqslant B \leqslant 60\ \text{T}$. Computations are carried out for spin polarized electronic systems, with total spin $M^{e}_{s} = N_e/2$, which contribute to the LHCP spectra. The energies of the incompletely polarized states with $M^{e}_{s} = N_e/2 - 1$, entering the RHCP spectra, are obtained by adding the corresponding Zeeman shifts.

### 3.1. Binding energies of excitonic complexes

We draw in Fig. 1 the g.s. energies, $\varepsilon$, coming from the diagonalization of $V_{\text{conf}} + V_{\text{coul}}$ in Eq. (1) as

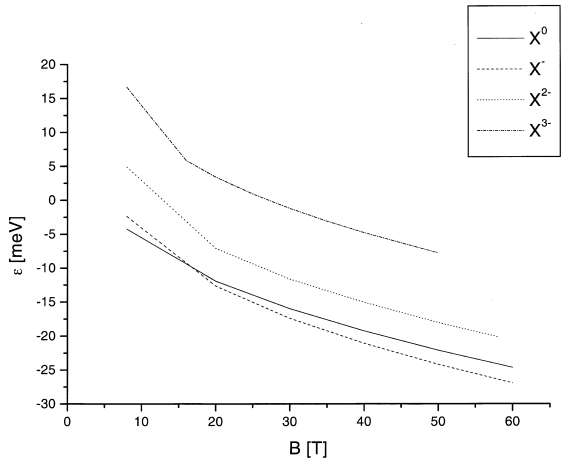


Fig. 1. g.s. energies of the excitonic $X^{N_e-}$ complexes, denoted also as $(N_e + 1, 1)$ in the main text.

a function of the applied magnetic field. The polarized systems $(N_e + 1, N_h) = (1, 1)$, $(2, 1)$ $(3, 1)$ and $(4, 1)$ are shown. The common notation for the excitonic systems $(1, 1)$ and $(2, 1)$ are $X^0$ and $X^-$, so that the charged complex $(4, 1)$ may be denoted $X^{3-}$. Note that the slopes of the $(2, 1)$, $(3, 1)$ and $(4, 1)$ curves are very similar. It means that the relative binding energies vary smoothly with $B$, and that the magnetic moments of these states take almost the same values. For example, $X^{3-}$ is 14.77 meV above $X^-$ at $B = 30$ T, and 14.29 meV above $X^-$ at $B = 50$ T.

The total angular momenta in the g.s. is a constant, independent of $B$, in the smallest systems. It is $M_{gs} = 0$ in the exciton, and $M_{gs} = -1$ in the triplet $X^-$ at any $B$. The larger systems, however, undergo abrupt rearrangements at particular $B$ values. The interplay between g.s. rearrangements in the $(N_e, 0)$ and $(N_e + 1, 1)$ systems as $B$ is varied has direct consequences on absorption and luminescence, as will be seen below.

Note that, unlike pure electron systems, when holes are present the Hilbert space in a given $M = -|M_e| + M_h$ sector is not finite. We enlarged the included subspace until convergence is reached. For example, in the $(4, 1)$ system at $B = 40$ T, 2374 many-particle states (i.e. all of the states in $15 \leqslant |M_e| \leqslant 35$) are enough to reach convergence for the lowest energy eigenvalue in the $M = -15$ tower.

The low-lying energy levels of $X^{3-}$ at $B = 35$ T are shown in Fig. 2 as an example. Energy distances between the lowest adjacent levels are around 0.5 meV, the same as in the three-electron system at this value of the magnetic field.

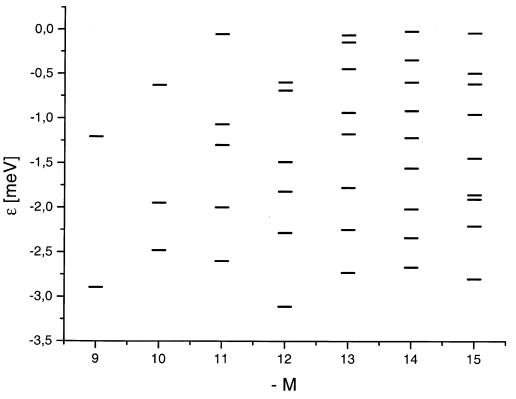


Fig. 2. Low-lying energy levels of the polarized $X^{3-}$ complex at $B = 35$ T.

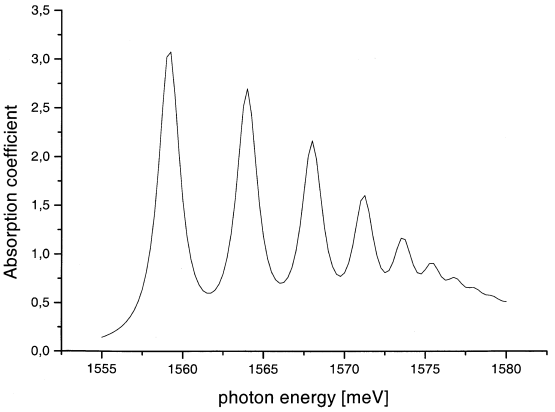


Fig. 3. Absorption coefficient of the neutral $(N_e = 0)$ qdot at $B = 40$ T.

### 3.2. Interband absorption

As previously stated, temperatures are low enough for absorption to proceed from the g.s. of the $N_e$-electron system. It means that spin flips should not be thermally induced, i.e. $T \ll 2$ K for $B > 8$ T.

We show in Fig. 3 the absorption coefficient for the $N_e = 0$ qdot at $B = 40$ T. The process under consideration, $(0, 0) \rightarrow (1, 1)$, goes through the $M = 0$ channel. The main properties of the curve drawn in Fig. 3,

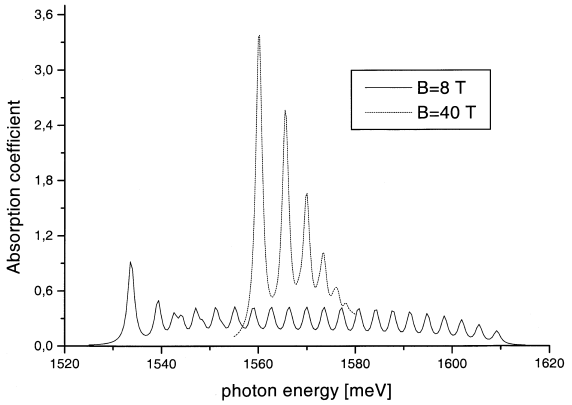


Fig. 4. Absorption coefficient of the $N_e = 1$ qdot at $B = 8$ and 40 T.

i.e. dominance of the exciton g.s. and monotony, are visible also at any other value of the magnetic field. The main effect of $B$ is to reinforce the dominance of the first line. The threshold for absorption is determined by the exciton g.s. energy, and the maximum dipole squared behaves like $B^{0.78}$.

The absorption coefficient of the negatively charged dot, $N_e = 1$, is shown in Fig. 4. The $(1, 0) \rightarrow (2, 1)$ process takes place in the $M = 0$ sector. At $B = 8$ T, a structure of isospaced bands is seen in the spectrum at higher energies. Most of these lines are suppressed already at $B = 40$ T. The threshold for absorption and maximum strength transition are determined by the lowest $X^-$ state in the $M = 0$ tower. As a function of $B$, we get $D^2 \sim B^{0.79}$ at the maximum.

The absorption thresholds for the smallest systems, $N_e = 0$ and 1, are smooth functions of $B$, signalling that the states entering the transition $(N_e, 0) \rightarrow (N_e + 1, 1)$ do not change qualitatively as $B$ is raised. For larger systems, however, there is an abrupt decrease in the threshold for fields around 10 T ("filling factor" near one), and small steps at higher fields. The steps are originated by the different rates of change of $M_{gs}$ in the $(N_e, 0)$ and $(N_e + 1, 1)$ systems (see Table 1). Let us consider, for example, the $(3, 0) \rightarrow (4, 1)$ process. For $B \leqslant 10$ T, the process goes from the g.s. of $(3, 0)$ to the excited states of $X^{3-}$ with $M = -3$. For $B > 10$ T, the g.s. of $(3, 0)$ moves to $M = -6$, a sector which contains the g.s. of $(4, 1)$. Thus, the threshold is lowered. Every time one of the systems rearranges, there is a step like change in the absorption threshold. The actual (experimental) profile is expected to be smoothed because of temperature effects.

Table 1
Ground-state orbital angular momentum in the $N_e = 2$ and 3 dots

| $B$ [$T$] | $M_{gs}(2, 0)$ | $M_{gs}(3, 1)$ | $M_{gs}(3, 0)$ | $M_{gs}(4, 1)$ |
|---|---|---|---|---|
| 8 | 1 | 3 | 3 | 6 |
| 16 | – | – | 6 | 6 |
| 20 | 3 | 3 | 6 | 9 |
| 25 | – | – | 9 | 9 |
| 30 | 3 | 3 | 9 | 12 |
| 35 | 5 | 3 | 12 | 12 |
| 40 | 5 | 5 | 12 | 15 |
| 45 | – | – | 15 | 15 |
| 50 | 7 | 5 | 15 | 18 |
| 58 | 7 | 7 | – | – |

Of course, not only threshold changes, but the whole spectrum is restructured. We show in Fig. 5 the absorption in the $N_e = 2$ dot ($X^{2-}$ formation) at $B = 8$ T and 50 T. At $B = 8$ T, the spectrum is similar to the $X^-$ spectrum. The added electron is placed in an outer orbit because the inner orbitals are filled. For higher fields, there is place for the new electron in the core region, but the minimization of energy causes a global restructuration of the charge density in the dot, as will be seen below. The added pair losses its identity. Notice that for $B > 10$ T there are two very distinct lines in the spectrum. One is the threshold (the transition to the lowest state of $(3, 1)$), and the second is the maximum, which is 7–4 meV above the threshold.

The dipole squared at maxima as a function of $B$ are drawn in Fig. 6. Besides lowest state rearrangements, there are manifestations of collective effects even in these small systems. A decrease of absorption in the $N_e = 2$ and 3 systems at "filling factors" $\nu \approx \frac{1}{2}$, $\frac{1}{3}$ and $\frac{1}{5}$ is evident from Fig. 6.

### 3.3. Magnetoluminescence

The second part of Fig. 5 shows the square of the dipole matrix elements corresponding to the luminescence of the $N_e = 2$ dot at $B = 40$ T. Only transitions starting from the g.s. of $(3, 1)$ are considered. Notice that the lowest state $(2, 0)$ gives the strongest line, approximately 50 times higher than the next one. This is the common situation in our luminescence calculations for any of the systems under study. The strongest line corresponds to the transition from the g.s. of

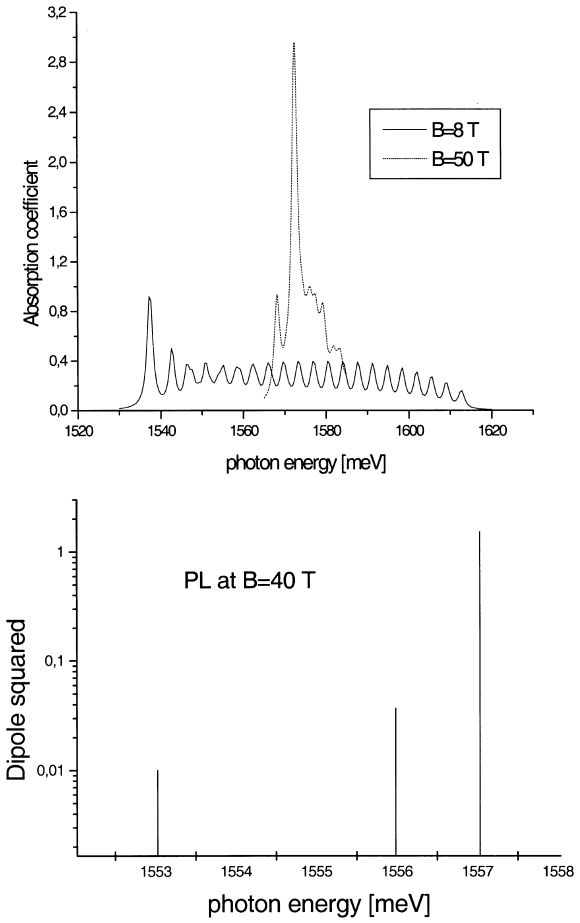


Fig. 5. Absorption and PL in the $N_e = 2$ dot.

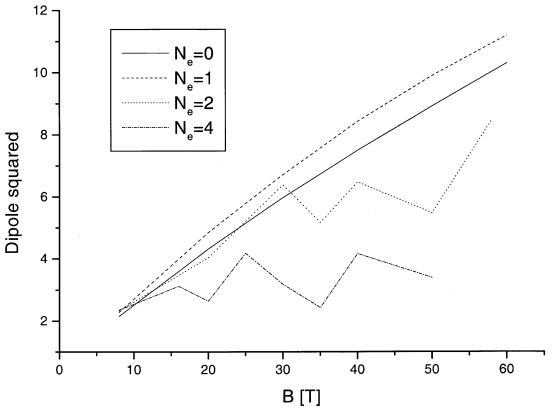


Fig. 6. Squared dipole matrix elements of the strongest absorption lines in the $N_e$-electron qdots vs. $B$.

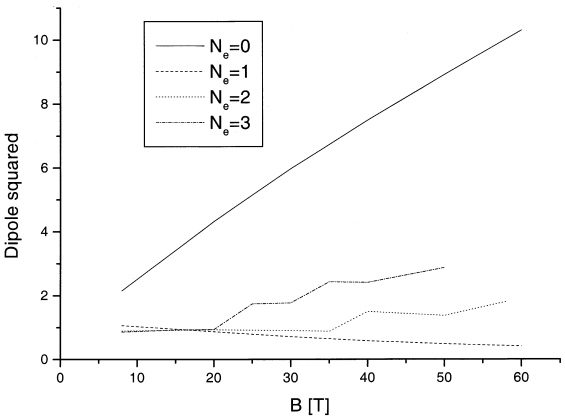


Fig. 7. Luminescence maxima in the $N_e$-electron qdots vs. $B$.

$(N_e + 1, 1)$ to the lowest state of $(N_e, 0)$ in the same angular momentum tower. The higher states of $(N_e, 0)$ give negligible contributions.

Luminescence in the $N_e = 0$, and 1 dots is monotonic with $B$ because the initial and final states participating in it are fixed. Exciton luminescence proceeds in the $M = 0$ channel, and $X^-$ luminescence in the $M = -1$ sector. In the latter case, the absorption and luminescence channels are different. With increasing $B$, the $X^0$ peak intensity increases, as in absorption, but the $X^-$ intensity decreases. We obtained $D^2 \sim \exp(-0.018B)$ the maximum.

For larger systems, the luminescence shows non-monotonic behaviour because of lowest state rearrangements and collective effects, as in absorption. As a rule, the channels for absorption and PL are different in these systems. The luminescence maxima as a function of $B$ are drawn in Fig. 7.

### 3.4. Charge densities

Electron and hole charge densities inside the dot for the relevant states participating in absorption and luminescence are presented in this section. For electrons we found more convenient to draw the difference $\rho'_e = \rho_e(N_e + 1, 1) - \rho_e(N_e, 0)$, which gives the density "added" to the dot.

Fig. 8 shows the final-state densities in the absorption situations discussed in Fig. 5. For the $N_e = 2$ dot

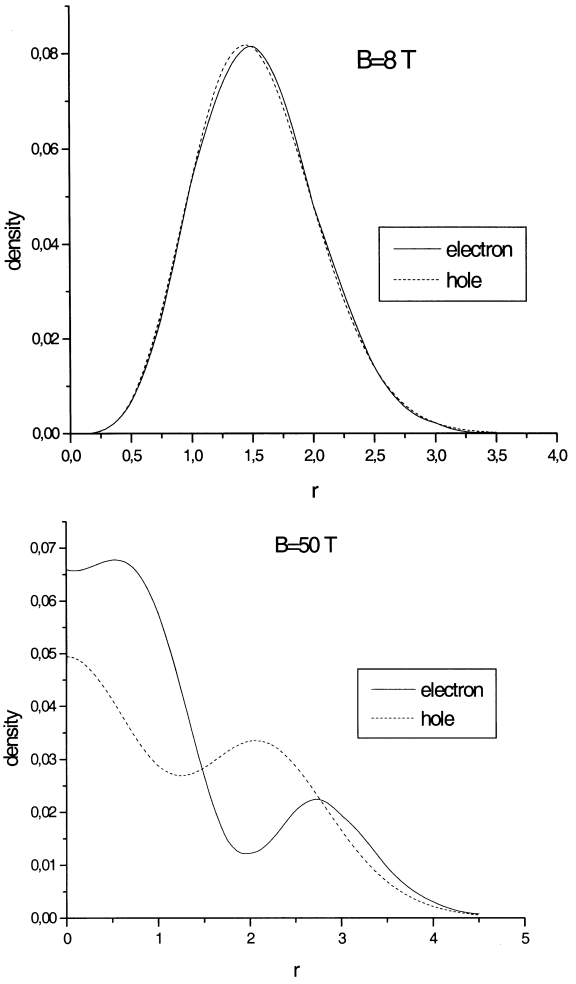


Fig. 8. Charge densities in final states with maximal absorption. The same cases as in Fig. 5 are considered.

at $B = 8$ T, the added electron and hole densities are almost identical. The exciton keeps its identity inside the dot. At $B = 50$ T, however, the added pair causes a redistribution of the charge density of the initial two-electron state.

On the other hand, as shown above, the relevant states participating in luminescence transitions are the g.s. of $(N_e + 1, 1)$ and the lowest state of the $N_e$-electron system in the same angular momentum sector. We show in Fig. 9 the densities of these states in the $N_e = 2$ dot at $B = 40$ T. These curves are typical. The exciton is annihilated from a distribution

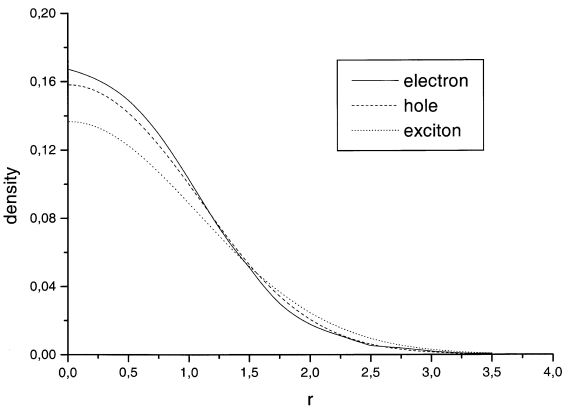


Fig. 9. Charge densities of the state with maximal oscillator strength in the luminescence of the $N_e = 2$ qdot at $B = 40$ T.

very similar to the isolated exciton g.s. (also shown in the figure for comparison).

## 4. Concluding remarks

We have studied few-electron systems and excitonic complexes (with one hole) in qdots under intense magnetic fields and low temperatures. In 1- and 2-electron qdots the g.s. angular momentum is independent of the magnetic field intensity. However, larger systems undergo abrupt rearrangements at particular $B$ values, a fact that is reflected in the optical absorption and PL.

We computed the interband optical properties of these systems. In absorption, the initial state is the polarized ground state of $N_e$ electrons (for temperatures $\ll 2$ K) and the final states are the states of $N_e + 1$ electrons and one hole. The main result of these computations is the nonmonotonic behaviour of the absorption maxima in the larger ($N_e = 2$ and 3) systems as the field is varied (Fig. 6). This result can be understood as a consequence of ground state rearrangements and collective effects. We have presented typical charge densities in support of this picture. We found a reduction of absorption at " filling factors" $\frac{1}{2}$, $\frac{1}{3}$ and $\frac{1}{5}$.

For luminescence events, we have considered the recombination from the g.s. of $N_e + 1$ electrons and a hole. At a given magnetic field intensity, the angular momentum of this state may be different from the $N_e$-electron g.s. angular momentum. Thus,

intrinsic absorption and luminescence may proceed through different channels. Of particular interest is that, opposite to the qwell case, the negatively charged exciton $X^-$ is bright in luminescence. This is a consequence of the qdot lateral confinement. Furthermore, for very high $B$ the $X^-$ complex recovers its dark character as compared with the other complexes here studied. On the other hand, the maximum of the recombination oscillator strength is a monotonic function of $B$ for qdots with 1 or 2 electrons and a hole, but it is nonmonotonic for qdots with more electrons, showing collective effects even in these small dots.

Although our calculations for finite systems with a smooth lateral confinement cannot be easily extrapolated to the infinite limit, our results suggest that many-body effects should be taken into account in the computation of the $X^-$ luminescence in a qwell. Whittaker and Shields [21] and Wojs et al. [22] have used a three-particle model for the $X^-$. This model is indeed useful at very high magnetic fields. At intermediate values of $B$, the magnetoexciton size, which is $\sim 2l_B \sim 50/\sqrt{B}$ nm, becomes comparable to the inter-electronic distance, around 20 nm for a typical carrier density of $1–2\times10^{11}$ cm$^{-2}$. Many-body effects should take care of observed dependence of the PL maximum with the filling factor.

We have not attempted a more sophisticated calculation in these systems because of the absence of experimental results for qdots in very intense magnetic fields. Nevertheless, our simple approach (1LL, one qwell subband, parabolic lateral confinement, unrealistic Zeeman energies and $z$-averaged Coulomb interactions) captures the essential physics and indicates the importance of collective effects even in small qdots.

## Acknowledgements

A.G. acknowledges support by the Caribbean Network for Theoretical Physics. E.M-P. acknowledges the Abdus Salam ICTP, where part of this work was done. The authors are grateful to C. Trallero-Giner for many useful discussions.

## References

[1] R.B. Laughlin, Phys. Rev. Lett. 50 (1983) 1395.
[2] J.K. Jain, R.K. Kamilla, in: O. Heinonen (Ed.), Composite Fermions, World Scientific, New York, 1998.
[3] S.M. Girvin, A.H. MacDonald, P.M. Platzman, Phys. Rev. B 33 (1986) 2481.
[4] T. Chakraborty, P. Pietilainen, The Quantum Hall Effects, Springer, New York, 1996.
[5] V.W. Scarola, K. Park, J.K. Jain, cond-mat/9910491.
[6] K. Park, J. Jain, cond-mat/9910460.
[7] A. Pinczuk et al., Phys. Rev. Lett. 70 (1993) 3983.
[8] H.D.M. Davies, J.C. Harris, J.F. Ryan, A.J. Turberfield, Phys. Rev. Lett. 78 (1997) 4095.
[9] A. Pinczuk et al., Proceedings of 12th International Conference on High Magnetic Fields in Phys. of Semiconductors, World Scientific, Singapore, 1997, p. 83.
[10] M. Kang, A. Pinczuk, B.S. Dennis, M.A. Eriksson, L.N. Pfeiffer, K.W. West, cond-mat/9911350.
[11] C.J. Mellor et al., Phys. Rev. Lett. 74 (1995) 2339.
[12] U. Zeitler et al., Phys. Rev. Lett. 82 (1999) 5333.
[13] A.J. Shields, M. Pepper, M.Y. Simmons, D.A. Ritchie, Phys. Rev. B 52 (1995) 7841.
[14] G. Finkelstein, H. Shtrikman, I. Bar-Joseph, Phys. Rev. B 53 (1996) R1709.
[15] A.J. Shields, J.L. Osborne, D.M. Whittaker, M.Y. Simmons, M. Pepper, D.A. Ritchie, Phys. Rev. B 55 (1997) 1318.
[16] Y. Kim, C.H. Perry, K.S. Lee, D.G. Rickel, Phys. Rev. B 59 (1999) 1641.
[17] M. Hayne, C.L. Jones, R. Bogaerts et al., Phys. Rev. B 59 (1999) 2927.
[18] Y. Kim, F.M. Muntcanu, C.H. Perry, D.G. Rickel, J.A. Simmons, J.L. Reno, Phys. Rev. B 61 (2000) 4492, 4731.
[19] J.J. Palacios, D. Yoshioka, A.H. MacDonald, Phys. Rev. B 54 (1996) R2296.
[20] I.V. Lerner, Yu.E. Lozovik, Zh. Eksp. Teor. Fiz. 80 (1981) 1488 [Sov. Phys. JETP 53 (1981) 763.
[21] D.M. Whittaker, A.J. Shields, Phys. Rev. B 56 (1997) 15 185.
[22] A. Wojs, J.J. Quinn, P. Hawrylak, cond-mat/0001327; cond-mat/0001328.
[23] R. Cingolani, R. Rinaldi, H. Lipsalen et al., Phys. Rev. Lett. 83 (1999) 4832.
[24] A. Wojs, P. Hawrylak, Phys. Rev. B 51 (1995) 10 880.
[25] A.H. MacDonald, G.C. Aers, Phys. Rev. B 29 (1984) 5976.
[26] O. Madelung, H. Schulz, H. Weiss (Eds.), Landolt-Börnstein Tables, Vol. 3/17a and 22a, Springer, Berlin, 1982.
[27] L.M. Roth, B. Lax, S. Zwerdling, Phys. Rev. 114 (1959) 90.
[28] A.J. Shields, M. Pepper, D.A. Ritchie, M.Y. Simmons, Adv. Phys. 44 (1995) 47.
[29] M. Seck, M. Potemski, P. Wyder, Phys. Rev. B 56 (1997) 7422.